Comparative ESR Studies on the Reducibility and Adsorbate Interactions of Paramagnetic Ni(I) in Synthetic Ferrierite and Mordenite

Hosun Choo,[†] Suk Bong Hong,[‡] and Larry Kevan*,[†]

Department of Chemistry, University of Houston, Houston, Texas 77204-5641, and Department of Chemical Technology, Taejon National University of Technology, Taejon 305-719, Korea

Received: October 4, 2000

The formation of monovalent nickel in NiNaK-ferrierite and its interaction with several adsorbates are compared to those of Ni(I) species in NiNaK-mordenite using electron spin resonance (ESR) spectroscopy. The ESR results show higher reducibility of Ni(II) in ferrierite upon thermal and hydrogen reduction. This is due to a lesser negative charge of the ferrierite framework. Dehydration at 573 K as well as hydrogen reduction at 573 K produces one Ni(I) species in both NiNaK-ferrierite and NiNaK-mordenite. However, Ni(I) species in these two materials show noticeable differences in the way they interact with several adsorbates. This suggests that the Ni(I) ions in these two materials are in different sites. The lesser accessibility of Ni(I) in ferrierite to larger adsorbate molecules leads to the assignment that Ni(I) is in a small ferrierite cage. The contrasting greater accessibility of Ni(I) in mordenite to adsorbates suggests a Ni(I) site in the large 12-ring channel in mordenite. The reduction of Ni(I) in mordenite to Ni(0) by methanol and pyridine further supports this location assignment.

Introduction

Transition-metal ions exchanged into pentasil-containing zeolites such as ferrierite and mordenite have been reported to exhibit high and stable activity in several catalytic reactions depending on the type of transition metal.[1−7] Co(II) ions at cationic sites in these materials are active sites for selective catalytic reduction of NO by methane in excess oxygen and for the selective ammoxidation of ethane to acetonitrile.[1,2] Cu(II) ions have been reported to be active sites in direct decomposition of NO to N_2 and O_2.[3,4] Ni(I) ions stabilized in several other zeolites were found to exhibit high catalytic activity in various reactions such as the dimerization of small olefins[5,6] and the selective conversion of methanol to ethane.[7] It is also known that their catalytic activities differ in different types of zeolites and are dependent on the concentration and location of transition-metal ions as well as on their accessibility to and coordination with adsorbate molecules. The principal methods that have been used to elucidate the catalytic function of transition-metal ions within zeolites are based on the adsorption of typical probe molecules and their interaction with active sites. While several studies have been reported on the location and coordination of copper[8,9] and cobalt ions[10,11] in pentasil zeolites, there is no available information on monovalent Ni(I) in these zeolites. This is probably due to the difficulty in the isolation and detection of Ni(I) species. Monovalent Ni(I) ions can be produced by reduction of Ni(II) after Ni(II) ions are incorporated into extraframework sites in zeolites by liquid-phase and solid-state ion exchange. The formation of Ni(I) ions in zeolites is highly sensitive to the reduction method and conditions, the amount of Ni(II) ions, and the ion-exchange method employed. Therefore, it is important to determine the optimum conditions for generating a high amount of Ni(I) ions without forming Ni(0). Ni(I) ions have been stabilized previously in several other zeolites and silicoaluminophosphate materials.[12−14]

Mordenite and ferrierite are naturally occurring silica-rich aluminosilicates with channel systems.[15,16] They are structurally similar and are classified in the mordenite group, which includes mordenite, ferrierite, epistilbite, bikitaite, and dachiardite.[17] They have various ion-exchangeable cations to balance their negative framework charge. Ferrierite has an orthorhombic framework forming a two-dimensional channel system with spherical cages.[17,18] This channel system consists of a 10-membered ring channel intersecting perpendicularly with an 8-membered ring channel. Mordenite has a 1-dimensional, 12-membered ring channel system with side pockets involving 8-membered ring channels.[19,20] The main differences between mordenite and ferrierite are (i) the lower Si/Al ratio in mordenite, which may affect the reducibility of Ni(II), and (ii) lesser accessibility to cations situated in the side pockets of mordenite compared to cations located in ferrierite cages. The characteristic channel systems of mordenite and ferrierite, their high thermal stability, and their large ion-exchange capacity make them potentially interesting catalysts.

In this study, we have hydrothermally synthesized NaK-mordenite and NaK-ferrierite and have introduced Ni(II) by ion exchange. The formation of paramagnetic Ni(I) and its interaction with various adsorbates have been studied to deduce probable locations of Ni(I) ions and to provide a better understanding of the activity of Ni(I) in ferrierite and mordenite. We also discuss comparative electron spin resonance (ESR) results on the reducibility of Ni(II) to Ni(I) between ferrierite and mordenite.

Experimental Section

Synthesis. NaK-ferrierite was synthesized hydrothermally using pyrrolidine as the organic template.[21] This sample was calcined at 823 K in O_2 overnight to remove the organic template.

[†] University of Houston.
[‡] Taejon National University of Technology.

10.1021/jp0036341 CCC: $20.00
Published on Web 02/15/2001

Single-phase NaK-mordenite was hydrothermally synthesized.[18] The following chemicals were used without further purification: 6 N NaOH solution, 6 N KOH solution, dried aluminum hydroxide, $Al(OH)_3$ (USP, Pfaltz & Bauer Inc.), colloidal silica (Ludox LS, Aldrich). The synthesis was carried out in stainless steel autoclaves with Teflon liners at autogenous pressure. The molar composition of the reaction mixture was 0.9 NaOH:0.9 KOH:1 $Al(OH)_3$:5.5 SiO_2. In a typical synthesis, 2.34 g of dried aluminum hydroxide was added to a mixture of 4.5 mL of 6 N NaOH and 4.5 mL of 6 N KOH. After the resultant mixture was stirred for 1 h, 27.3 mL of colloidal silica was added slowly, and the mixture was further stirred for 1 h. The pH of the final mixture was 12.4. This gel was put into a 100 cm^3 static autoclave and was annealed at room temperature for 1 h before being heated at 453 K for 96 h. After crystallization, the product was washed with water and dried at 343 K overnight.

Ni^{II}NaK-mordenite and Ni^{II}NaK-ferrierite were prepared by liquid-state ion exchange with various concentrations of $NiCl_2 \cdot 6H_2O$ (Aldrich) at room temperature for 24 h. The chemical compositions of these final ion-exchanged samples are $Ni_{0.004}$ $Na_{0.012}K_{0.058}$ $[Al_{0.11}Si_{1.0}O_2]$ for NiNaK-ferrierite and $Ni_{0.004}Na_{0.013}K_{0.053}$ $[Al_{0.12}Si_{0.85}O_2]$ for NiNaK-mordenite on the basis of electron microprobe analyses.

Sample Treatment and Measurement. Powder X-ray diffraction (XRD) patterns were recorded on a Siemens D5000 X-ray diffractometer using Cu Kα radiation. Thermogravimetric analyses (TGA) and differential thermal analysis (DTA) were carried out in N_2 on a Dupont 957 thermal analyzer at a heating rate of 10 °C/min. Chemical analyses of the samples were carried out by electron microprobe analysis on a JEOL JXA-8600 spectrometer. For the various ESR measurements, hydrated samples were loaded into 3 mm o.d. by 2 mm i.d. Suprasil quartz tubes and evacuated at 298 K for 24 h. To study the behavior of Ni(II) as a function of dehydration, the samples were slowly heated under vacuum ($<10^{-4}$ Torr) from room temperature to 373, 473, and 573 K. This procedure accomplishes thermal reduction. To see whether any Ni(I)$-H_2$ complexes are formed by hydrogen reduction, dehydrated samples after the following activation process were also exposed to dry hydrogen at room temperature and subsequently heated to various temperatures from 298 to 623 K for various durations. An activation treatment involved heating dehydrated samples in 500 Torr of dry oxygen at 623 K for 5 h followed by evacuation at the same temperature overnight to reoxidize any Ni(I) formed during dehydration. ESR spectra were then recorded at 77 K to detect the formation of any Ni(I) species. To study Ni(I) interactions with various adsorbates, reduced samples were exposed to the room temperature vapor pressure of CH_3OD (Stohler Isotope Chemicals) and pyridine (Cambridge Isotopes), 8 Torr of ^{13}CO (Cambridge Isotopes), and 20 Torr of ^{12}CO (Trigas), C_2D_4 (Cambridge Isotopes), and ND_3 (Stohler Isotope Chemicals). These samples with adsorbates were frozen in liquid nitrogen and sealed for ESR. In the case of NO treatment, activated samples were directly contacted with 20 Torr of NO at 298 K for 2 min.

The ESR spectra were recorded at 77 K with a Bruker ESP 300 X-band spectrometer. The magnetic field was calibrated with a Varian E-500 gaussmeter. The microwave frequency was measured by a Hewlett-Packard HP 5324A frequency counter.

Results

X-ray Powder Diffraction. Figure 1 shows the powder XRD patterns of as-synthesized NaK-mordenite and NaK-ferrierite. These patterns match well with the XRD patterns of naturally occurring mordenite and ferrierite, respectively.[18] No loss in crystallinity was observed by XRD after as-synthesized ferrierite was calcined by heating at 823 K overnight to remove the organic template.

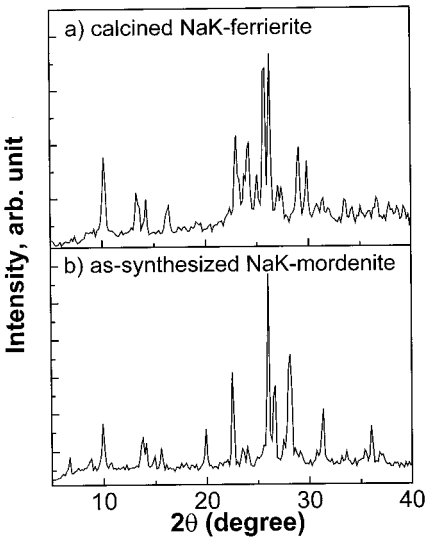

Figure 1. X-ray powder diffraction patterns of (a) calcined NaK-ferrierite and (b) as-synthesized NaK-mordenite.

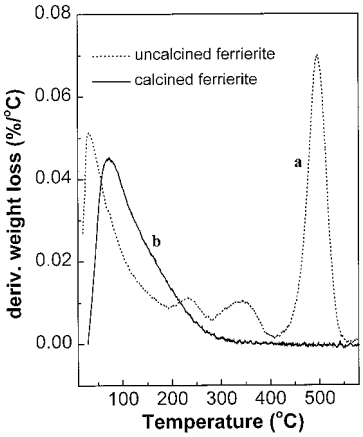

Figure 2. Thermogravimetric analysis curves in flowing nitrogen of as-synthesized NaK-ferrierite (a) before and (b) after calcination at 823.

Thermogravimetric Analysis. Figure 2 shows the TGA curves of as-synthesized NaK-ferrierite measured before and after calcination. The dashed TGA curve for uncalcined NaK-ferrierite shows four stages of weight loss around 50, 250, 350, and 500 °C. The first weight loss around 50 °C is assigned to the desorption of physically adsorbed water. Two peaks near 250 and 350 °C are assigned to desorption of the organic template. The observation of two peaks indicates that desorption of pyrrolidine takes place from two sites in ferrierite. The weight loss around 250 °C is possibly ascribed to the decomposition of organic templates in the main 10-membered ring channels. The weight loss at 350 °C is assigned to the decomposition of organic templates in 8-ring channels. These assignments are drawn from previous single-cyrstal XRD data on the location of pyridine in synthesized ferrierite.[22] An additional weight loss around 500 °C is possibly due to the decomposition of organic templates interacting with acid sites in ferrierite. The solid line TGA curve in Figure 2 for calcined NaK-ferrierite indicates that all organic templates were removed during the calcination process. This sample was used for ESR study. The TGA curve of as-synthesized mordenite shows a single peak around 100 °C due to the desorption of water molecules. No additional peaks

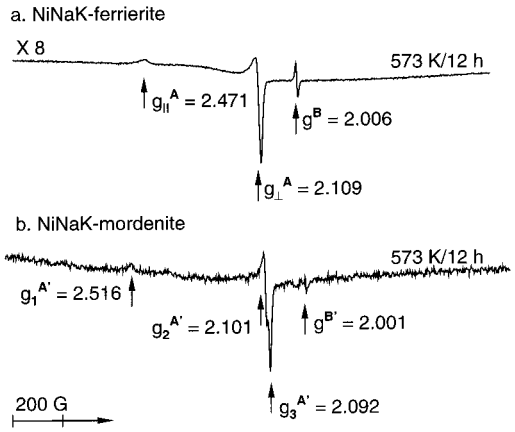

Figure 3. ESR spectra at 77 K after dehydration at 573 K for 12 h of (a) NiNaK-ferrierite and (b) NiNaK-mordenite.

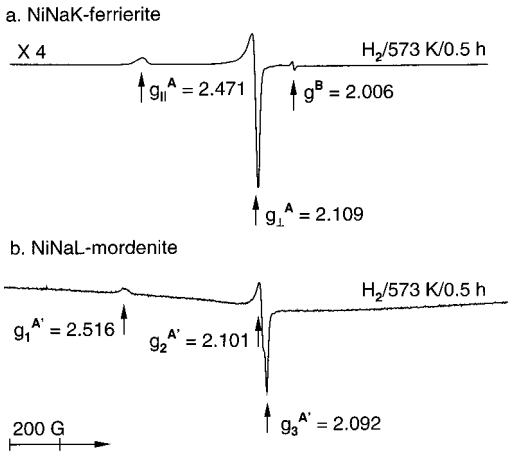

Figure 4. ESR spectra at 77 K after hydrogen reduction at 573 K for 0.5 h of (a) NiNaK-ferrierite and (b) NiNaK-mordenite.

are observed, since mordenite was synthesized without using an organic template.

ESR Measurements. Hydrated mordenite and ferrierite do not show any ESR signal at 77 K. Thus, the nickel ions exist as Ni(II), which is ESR silent. Figure 3 shows the ESR spectra of Ni^{II}NaK-ferrierite and Ni^{II}NaK-mordenite dehydrated at 573 K for 12 h. Dehydration at this temperature leads to the formation of two paramagnetic species denoted A and B in NiNaK-ferrierite and A′ and B′ in NiNaK-mordenite. Species A in NiNaK-ferrierite has axial symmetry with $g_{\parallel}^{A} = 2.471$ and $g_{\perp}^{A} = 2.109$, while species A′ in NiNaK-mordenite has slight rhombic symmetry with $g_1^{A'} = 2.516$, $g_2^{A'} = 2.101$, and $g_3^{A'} = 2.092$. Species A and A′ are assigned to isolated Ni(I) ions generated by thermal reduction in ferrierite and mordenite, respectively. The ESR signal intensity for Ni(I) species A produced in NiNaK-ferrierite is substantially higher than that of species A′ in NiNaK-mordente, suggesting higher reducibility of Ni(II) in ferrierite. Species B and B′ with ESR parameters of $g^{B} = 2.006$ and $g^{B'} = 2.001$ have been observed in several other zeolites and SAPO materials where they were assigned to an oxygen radical.[23,24] This assignment is supported by the observation that the intensities of species B and B′ increase upon adsorption of oxygen and readily decrease by subsequent evacuation of oxygen.

Figure 4 shows the ESR spectra of Ni^{II}NaK-ferrierite and Ni^{II}NaK-mordenite obtained after hydrogen reduction at 573 K for 0.5 h. Species A and A′ are also generated by hydrogen reduction of NiNaK-ferrierite and NiNaK-mordenite, respectively. They appear with the much stronger intensity than the corresponding signal intensity for species A and A′ produced by thermal reduction. The *g* values of species A are similar to those reported previously for Ni(I) in NiAPSO-5,[13] NiNaK-clinoptilolite,[25] and NiH-SAPO-41[26] and are slightly lower in comparison to those of Ni(II)-exchanged X and Y zeolites.[27,28] The rhombic symmetry of species A′ observed after thermal or hydrogen reduction of NiNaK-mordenite has not been reported earlier in other zeolites or SAPO materials.

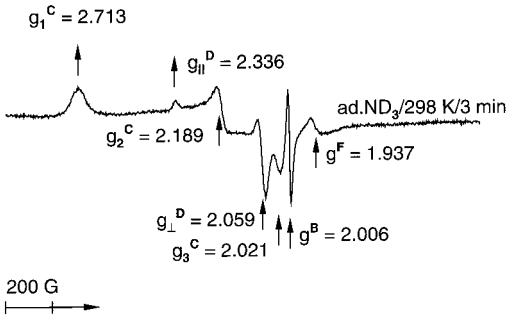

Figure 5. ESR spectra at 77 K of NiNaK-ferrierite after 20 Torr of ND_3 adsorption on a reduced sample at 298 K for 3 min.

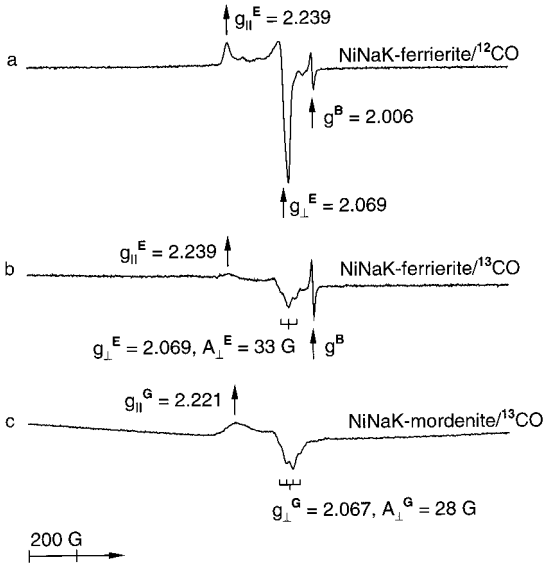

Figure 6. ESR spectra at 77 K after 20 Torr of ^{12}CO adsorption on reduced NiNaK-ferrierite at 298 K for 1 h (a) and after 8 Torr of ^{13}CO adsorption at 298 K for 1 h on reduced (b) NiNaK-ferrierite and (c) NiNaK-mordenite.

Adsorbate Interactions. Adsorption of ND_3 at room temperature on thermally reduced NiNaK-ferrierite produces two distinct new species, rhombic species C and axial species D, along with an isotropic radical species at $g^{B} = 2.006$ and a defect species at $g^{F} = 1.937$ (Figure 5). Species C is dominant with $g_1^{C} = 2.713$, $g_2^{C} = 2.189$, and $g_3^{C} = 2.021$. Species D has $g_{\parallel}^{D} = 2.336$ and $g_{\perp}^{D} = 2.059$. These species are assigned to two Ni(I)$-(ND_3)_n$ complexes located within the ferrierite structure. The behaviors of these species with respect to evacuation are different. Species C remains with almost the same intensity whereas the intensity of species D decreases upon evacuation of ammonia at 298 K for 15 min. Species F has been reported in H-SAPO-5 and Ni(II)-exchanged SAPO materials and was tentatively assigned to a nonspecific framework defect.[13]

The interaction of CO with Ni(I) in NiNaK-ferrierite and NiNaK-mordenite is shown in Figure 6. When 20 Torr of ^{12}CO (^{12}CO has zero nuclear spin) is adsorbed on a thermally reduced sample at 298 K for 1 h, Ni(I) species A disappears immediately

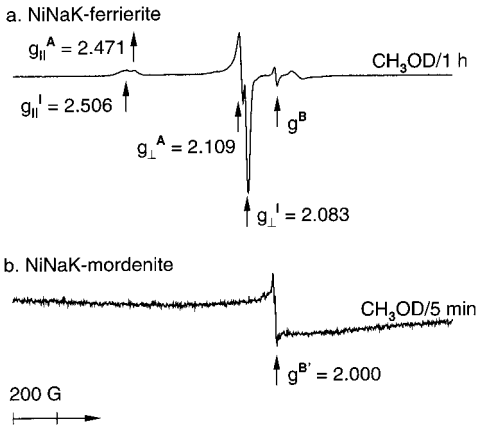

Figure 7. ESR spectra at 77 K after adsorption of CH_3OD at 298 K (a) for 1 h on reduced NiNaK-ferrierite and (b) for 5 min on reduced NiNaK-mordenite.

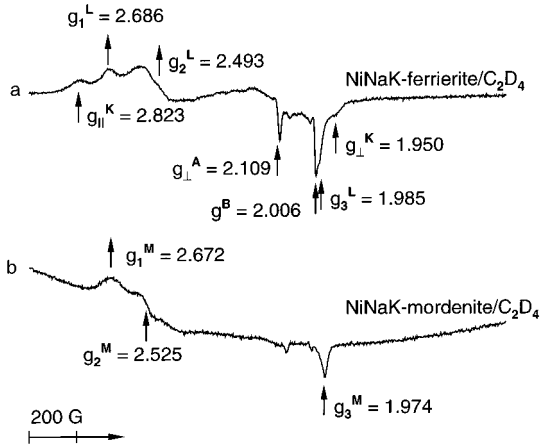

Figure 8. ESR spectra at 77 K after adsorption of C_2D_4 at 298 K for 3 min on reduced (a) NiNaK-ferrierite and (b) NiNaK-mordenite.

with the formation of a single new species, E (Figure 6a). Species E has axial symmetry with $g_{\|}^{E} = 2.239$, $g_{\perp}^{E} = 2.069$. When 8 Torr of ^{13}CO is added instead of ^{12}CO, the ESR spectrum (Figure 6b) shows a more complex pattern with a resolved hyperfine splitting of the $g_{\perp}$ component, $A_{\perp}^{E} = 33$ G. The analysis of this hyperfine structure leads to the assignment of species E to a Ni(I)$-(CO)_2$ complex. Similarly, adsorption of 8 Torr of ^{13}CO on reduced NiNaK-mordenite at 298 K for 1 h generates new species G with $g_{\|}^{G} = 2.221$ and $g_{\perp}^{G} = 2.067$, and the ^{13}C hyperfine interaction gives a quartet feature of the $g_{\perp}$ component and $A_{\perp}^{G} = 28$ G. Species G is assigned to a Ni(I)$-(CO)_3$ complex on the basis of the ^{13}C hyperfine structure.

Figure 7 shows the ESR spectra of NiNaK-ferrierite and NiNaK-mordenite observed after adsorption of methanol on thermally reduced samples at 298 K for different durations. Adsorption of CH_3OD on thermally reduced Ni^{I}NaK-ferrierite for 1 h generates single new species I with $g_{\|}^{I} = 2.506$ and $g_{\perp}^{I} = 2.083$, while Ni(I) species A still remains, indicating that only a part of Ni(I) species A is coordinated with methanol to give a new species, I, shown in Figure 7a. Ni(I) species A disappears completely upon annealing the methanol-adsorbed sample at 298 K for a longer time. ESR signals similar to those of species I, a Ni(I)$-(CH_3OD)_n$ complex, have been reported in previous NiCa-X zeolite and SAPO materials.[13,27]

The interaction of Ni(I) species A′ with CH_3OD in NiNaK-mordenite is different from that observed in NiNaK-ferrierite. Adsorption of methanol on NiNaK-mordenite at 298 K for 5 min causes Ni(I) species A′ to disappear completely but does not show any new ESR signal due to the formation of a Ni(I) complex with methanol. The broad baseline seen in NiNaK-mordenite after methanol adsorption is indicative of the formation of Ni(0) clusters, indicating that Ni(I) species A′ is further reduced to Ni(0) by methanol. This difference suggests that Ni(I) species A′ in NiNaK-mordenite is situated in a site which interacts more strongly with methanol compared to that of Ni(I) species A in NiNaK-ferrierite. Behavior similar to that of mordenite with respect to methanol adsorption has been observed in Pd(II)-exchanged K-L and H-ρ zeolites[29,30] and SAPO materials,[31,32] where adsorption of methanol leads to the formation of palladium clusters showing a broad isotropic signal ($g \approx 2.2$). This was mainly attributed to the location of Pd(II) and Pd(I) in the main large channels of these materials where Pd ions are readily reduced to Pd(0) by methanol.

Parts a and b of Figure 8 show the ESR spectra obtained after ethylene adsorption on reduced NiNaK-ferrierite and NiNaK-mordenite. When 20 Torr of ethylene is adsorbed on the thermally reduced NiNaK-ferrierite at 298 K for 3 min, two new species, denoted K and L, are observed, with a fraction of Ni(I) species A not interacting with ethylene. Species L has rhombic symmetry with $g_1^{L} = 2.686$, $g_2^{L} = 2.493$, and $g_3^{L} = 1.985$, and species K has axial symmetry with $g_{\|}^{K} = 2.823$ and $g_{\perp}^{K} = 1.950$. Rhombic species with ESR parameters similar to those of species L have been reported in NiCa-X[27] and NiNaK-clinoptilolite[25] and were assigned to Ni(I)$-(C_2D_4)_n$ complexes, but species K has not been observed previously. The assignment of species K to a Ni(I)$-(C_2D_4)_n$ complex is based on the fact that, along with species L, the intensity of species K decreases upon annealing at both 298 and 353 K. The formation of two species, K and L, indicates two Ni(I)$-(C_2D_4)_n$ complexes situated at two different sites within the ferrierite structure. On the other hand, adsorption of ethylene on Ni^{I}NaK-mordenite leads Ni(I) species A′ to disappear completely with the simultaneous formation of the new species M, indicating that all Ni(I) species A′ immediately interacts with ethylene to form a Ni(I)$-(C_2D_4)_n$ complex. Species M has $g_1^{M} = 2.672$, $g_2^{M} = 2.525$, and $g_3^{M} = 1.974$.

The ESR spectra obtained after adsorption of butene and pyridine on thermally reduced NiNaK-ferrierite do not show any new signals due to interactions of Ni(I) species A with butene and pyridine. This suggests that Ni(I) species A is situated at a site in ferrierite which is not accessible to butene and pyridine. On the other hand, adsorption of pyridine on reduced Ni^{I}NaK-mordenite leads to the formation of single species N with $g_1^{N} = 2.142$, $g_2^{N} = 2.094$, and $g_3^{N} = 2.070$, indicating that Ni(I) species A′ immediately coordinates with pyridine to form a Ni(I)$-(C_5D_5N)_n$ complex. This supports the Ni(I) species A′ in mordenite being situated at a site which is accessible to pyridine. The observation of a broad baseline for the corresponding spectrum suggests that pyridine possibly also reduces part of the Ni(I) to Ni(0). This is supported by the fact that the baseline broadens more as the annealing time increases.

Figure 9 shows the spectra recorded at 77 K after NO adsorption on NiNaK-ferrierite and NiNaK-mordenite dehydrated and oxidized prior to NO treatment. Adsorption of NO on Ni^{II}NaK-ferrierite produces two paramagnetic species, denoted R and B, respectively. Species R has a rhombic symmetry with $g_1^{R} = 2.347$, $g_2^{R} = 2.234$, and $g_3^{R} = 2.181$ and is assigned to a Ni(I)$-NO^{+}$ complex formed by the reduction of Ni(II) by NO. This assignment is based on the observations that species R is produced only with samples containing Ni(II) and that the intensity of this species is dependent on the Ni(II) amount ion-exchanged into ferrierite. The other species B found

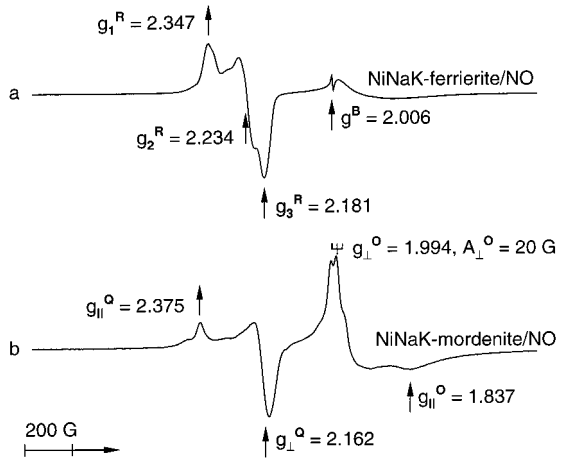

Figure 9. ESR spectra at 77 K after adsorption of NO at 298 K for 2 min on activated (a) Ni^{II}NaK-ferrierite and (b) Ni^{II}NaK-mordenite.

in NiNaK-ferrierite after adsorption of NO has been observed throughout the adsorption experiments with various molecules and is already assigned to an oxygen radical species.

For NO adsorption on NiNaK-mordenite, Figure 9b shows two species, Q and O. Species Q has axial symmetry with $g_{||}^Q = 2.375$ and $g_\perp^Q = 2.162$ and is assigned to a Ni(I)$-NO^+$ complex. Species O has $g_{||}^O = 1.837$ and a perpendicular component $g_\perp^O = 1.994$ split into a triplet with hyperfine splitting $A_\perp^O = 20$ G. These lines arise from hyperfine interaction of the odd electron of NO with a ^{14}N nucleus ($I = 1$). The *A* splitting as well as the principal *g* values of species O are very similar to those of NO radical species reported in several zeolites after NO adsorption.[33,34]

Table 1 summarizes the ESR parameters assigned to the various Ni(I) species observed in NiNaK-ferrierite and NiNaK-mordenite and their assignments.

Discussion

Ferrierite is a medium-pore zeolite whose framework is composed of alternating SiO_4 and AlO_4 tetrahedra with a Si/Al ratio of 9.1. Mordenite is classified as a large-pore zeolite with 12-ring channels and a Si/Al ratio of 7.1. Structural models of ferrierite and mordenite are shown in Figure 10. Ferrierite has a 2-dimensional channel system composed of 10-membered ring channels (4.2 × 5.4 Å) and 8-membered ring channels (3.5 × 4.8 Å)[17,18] which intersect perpendicularly. The 8-membered ring channel contains a spherical cavity, called a ferrierite cage, formed by the intersection of an 8-ring channel with a 6-ring channel and a 5-ring channel. This ferrierite cage has an 8-ring opening of 3.5 Å. Similarly, the framework of mordenite is based on 5-membered ring building units that are stacked in columns parallel to the *c*-axis.[19,20] The connection of these columns of 5-membered rings forms a 12-membered ring channel (6.5 × 7.0 Å) and an elliptical 8-membered ring channel (2.6 × 5.7 Å) running along the *c*-axis as shown in Figure 10b. These parallel channels are interconnected via small side pockets of 2.9 Å. These side pockets are not aligned along the *a*-axis, so no channel from them is formed along the *a*-axis.

Parts a and b of Figure 11 show the possible cation sites in dehydrated ferrierite and mordenite based on the cation sites identified by single-crystal X-ray diffraction of dehydrated natural ferrierite and mordenite, respectively.[35,36] Site A is located in the plane of a deformed 6-membered ring in the ferrierite cage. Cations in this site are coordinated to six framework oxygens. Site C corresponds to cations located in the 8-ring channels. The cation coordination in this site is not known. This site is occupied only by divalent cations. Site D is created by an 8-membered ring at the intersection of the 8-ring and 10-ring channels. Cations are placed in the ring plane, and the specific position of a cation and the number of coordinated framework oxygens depend on the metal ion radius. Site E is located in a main channel of ferrierite, and the cations are coordinated with four framework oxygens creating a rectangle in the channel wall. Cation sites and their coordinations found in dehydrated mordenite are the same as those in ferrierite. Site D is located in the plane of the 8-ring opening of the mordenite side pocket to a main channel. An additional site, B, is identified in dehydrated mordenite in an 8-ring channel of a mordenite side pocket. The detailed position and number of coordinated oxygens depend on the cation radius as for site D. Sites A−C are in side pockets of mordenite, while sites D and E are in a main 12-ring channel of mordenite.

Both thermal reduction and hydrogen reduction of NiNaK-ferrierite produce a single isolated Ni(I) ion, denoted as A, which results from reduction of Ni(II) to Ni(I). Similarly, a single isolated Ni(I) species, denoted as A′, is observed by thermal and hydrogen reduction of NiNaK-mordenite. However, the natures of these Ni(I) species A and A′ observed in ferrierite and mordenite differ in some ways. An isolated Ni(I) species in ferrierite shows axial symmetry with ESR parameters similar to those of isolated Ni(I) ions observed in other zeolites and SAPO materials,[24−27] while Ni(I) species A′ in mordenite shows rhombic symmetry. Rhombic symmetry of an isolated nickel

TABLE 1: ESR *g* Values of Paramagnetic Species Produced in NiNaK-ferrierite (NiNaK-fer) and NiNaK-mordenite (NiNaK-mor) after Reduction and Adsorbate Interactions

matrix	adsorbate	assignment	$g_{||}$ or g_1	$g_\perp$ or g_2	g_3	species
NiNaK-fer	none	Ni(I)	2.471	2.109		A
NiNaK-mor	none	Ni(I)	2.516	2.101	2.092	A′
NiNaK-fer	H_2	Ni(I)	2.471	2.109		A
NiNaK-mor	H_2	Ni(I)	2.516	2.101	2.092	A′
NiNaK-fer	ND_3	Ni(I)$-(ND_3)_n$	2.713	2.189	2.021	C
NiNaK-fer	ND_3	Ni(I)$-(ND_3)_n$	2.336	2.059		D
NiNaK-fer	CO	Ni(I)$-(CO)_2$	2.239	2.069		E
NiNaK-mor	CO	Ni(I)$-(CO)_3$	2.221	2.067		G
NiNaK-fer	CH_3OD	Ni(I)$-(CH_3OD)_n$	2.506	2.083		I
NiNaK-fer	C_2D_4	Ni(I)$-(C_2D_4)_n$	2.823	1.950		K
NiNaK-fer	C_2D_4	Ni(I)$-(C_2D_4)_n$	2.686	2.493	1.985	L
NiNaK-mor	C_2D_4	Ni(I)$-(C_2D_4)_n$	2.672	2.525	1.974	M
NiNaK-mor	C_5D_5N	Ni(I)$-(C_5D_5N)_n$	2.142	2.094	2.070	N
NiNaK-fer	NO	Ni(I)$-NO^+$	2.347	2.234	2.181	R
NiNaK-mor	NO	Ni(I)$-NO^+$	2.375	2.162		Q
NiNaK-mor	NO	NO radical	1.837	1.994		O

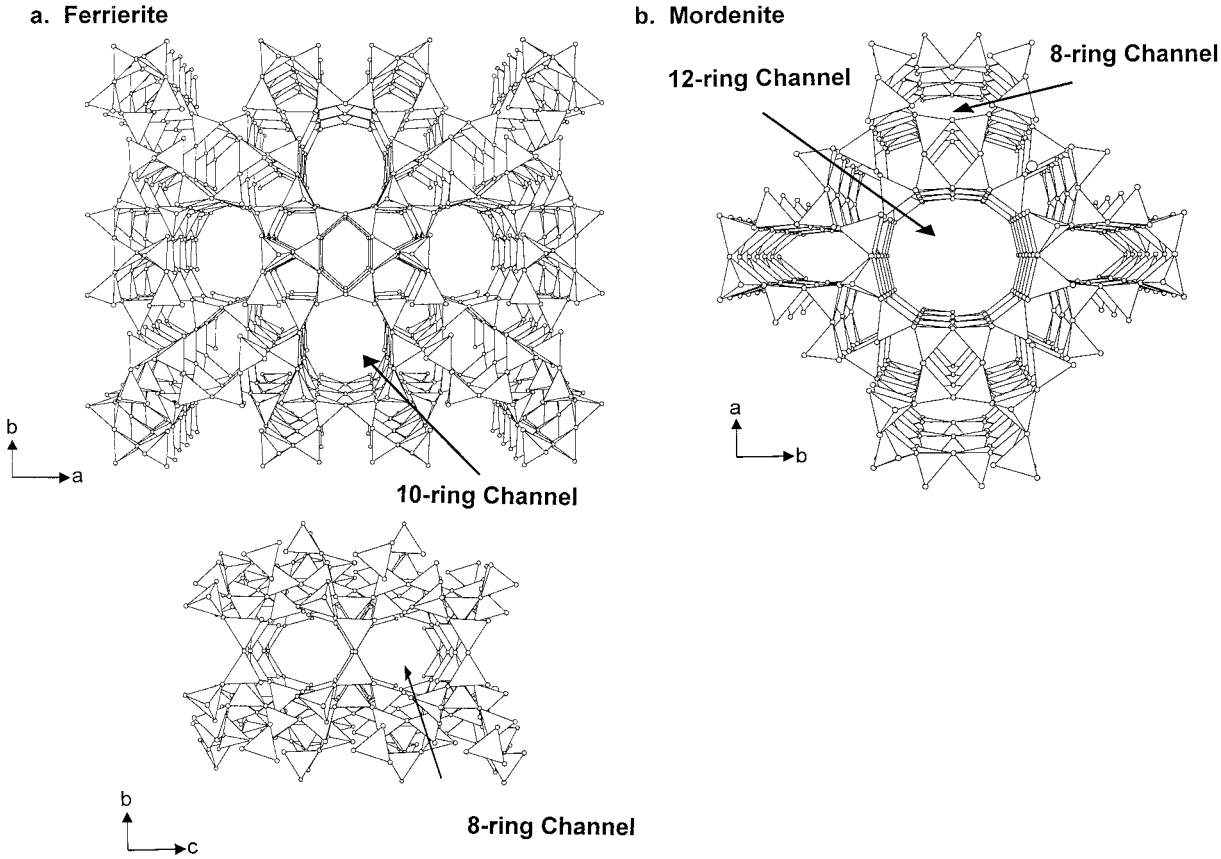

Figure 10. Structural models of (a) ferrierite and (b) mordenite viewed along the *c*-axis. The corner of a tetrahedron represents a framework oxygen. Al and Si atoms are located at the centers of the tetrahedra.

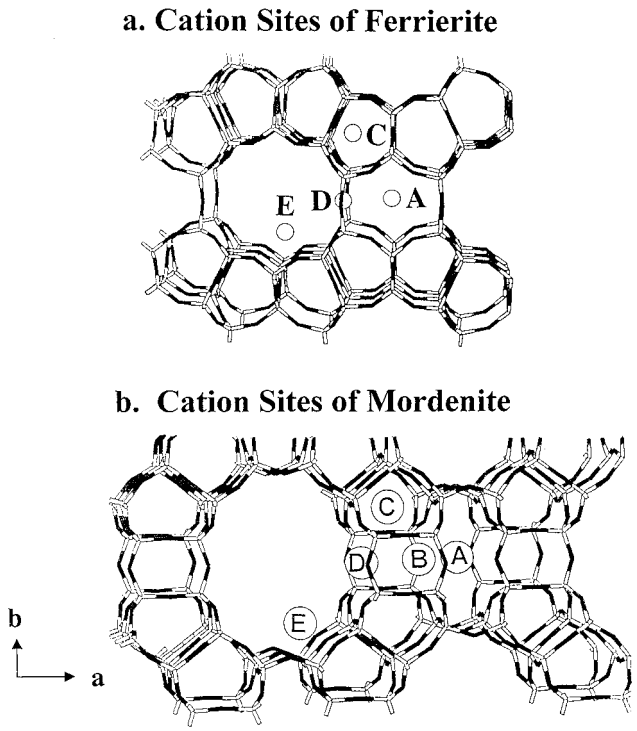

Figure 11. Possible cation sites and their designations in (a) ferrierite and (b) mordenite. Adapted from refs 10 and 11.

ion is unusual in microporous oxide materials.[23−28] Furthermore, the interaction of Ni(I) species A and A′ with various adsorbate molecules is substantially different between ferrierite and mordenite. This can be attributed to a difference in the environment experienced by Ni(I) in these two materials.

Molecules smaller than methanol, such as ammonia and CO, immediately interact with all of Ni(() species A in NiNaK-ferrierite to form complexes. Adsorption of ammonia leads to the formation of two Ni(I)−$(ND_3)_n$ complexes. Upon evacuation of ammonia at room temperature, one species decreases its intensity while the other remains unchanged. This suggests that there are two Ni(I)−$(ND_3)_n$ complexes in two different environments, one being in a more accessible site than the other. Adsorption of CO on reduced NiNaK-ferrierite leads to the formation of Ni(I)−$(CO)_2$, while CO adsorption on mordenite produces Ni(I)$(CO)_3$. In contrast, adsorption of methanol or ethylene on reduced NiNaK-ferrierite shows that a fraction of Ni(I) species A does not interact with methanol or ethylene. But, the unreacted species A then interacts with methanol or ethylene after annealing at room temperature for some time. The observation that Ni(I) species A interacts slowly with methanol and ethylene suggests that it is located at a site which is less accessible to methanol and ethylene in comparison to smaller adsorbates such as ammonia and carbon monoxide.

The behavior of NiNaK-mordenite with respect to methanol and ethylene adsorption is different from that of NiNaK-ferrierite. Adsorption of methanol on reduced NiNaK-mordenite leads to a broad ESR signal associated with the formation of Ni(0) clusters, indicating that Ni(I) species A′ in mordenite is not stable toward further reduction to Ni(0). Unlike NiNaK-ferrierite, adsorption of ethylene on reduced NiNaK-mordenite causes all Ni(I) species A′ to interact immediately with ethylene to form a Ni(I)−$(C_2D_4)_n$ complex. This observation supports again Ni(I) ions in NiNaK-mordenite after reduction occupying relatively accessible sites in comparison to those in NiNaK-ferrierite. This is presumably due to the different structures of these two zeolites. The difference in the stability of Ni(I) toward

methanol between NiNaK-ferrierite and NiNaK-mordenite reflects Ni(I) species A being in different sites in ferrierite and mordenite and the site in mordenite being less stable.

Adsorption of butene and pyridine on thermally reduced NiNaK-ferrierite and NiNaK-mordenite provides further information about the location of Ni(I) species A and A′ in these materials. The fact that no new ESR signal is observed upon adsorption of butene and pyridine in ferrierite indicates that Ni(I) species A does not interact with them and is located at a site inaccessible to benzene and pyridine. Thus, sites A and D within the ferrierite cage are probable sites for Ni(I) species A in ferrierite. However, cations in site D can migrate to a main 10-ring channel where they can interact with butene and pyridine. Thus, Ni(I) species A in ferrierite is most likely located in site A in a ferrierite cage. This assignment is consistent with the observation that Ni(I) species A in ferrierite is stable toward methanol adsorption.

For NiNaK-mordenite, adsorption of pyridine leads to the formation of a single Ni(I)$-(C_5D_5N)_n$ complex with a very broad baseline. The baseline becomes more broadened by annealing at room temperature, indicating further reduction to Ni(0) by pyridine. This behavior is the same as that observed after adsorption of methanol on reduced NiNaK-mordenite. The observation of a Ni(I)$-(C_5D_5N)_n$ complex in NiNaK-mordenite suggests that Ni(I) ions are situated at a site which is accessible to pyridine, probably site D or E in a main 12-ring channel.

Three sites of ion-exchanged Cu(II) in partially dehydrated Cu-mordenite have been previously determined from the analysis of room temperature single-crystal X-ray data.[37] One is in site A in an 8-ring channel where Cu(II) is coordinated with six framework oxygens. The other two sites, D and E, in a 12-ring channel seem more probable. Cu(II) in site D is coordinated with two framework oxygens, while Cu(II) in site E is coordinated with four framework oxygens.

A major factor which influences the stability of Ni(I) and its interaction with adsorbates is its location. Previous studies in Na-X and Na-Y zeolites have shown that during reduction Ni(I) has a high tendency to migrate into a small hexagonal prism (site SI) in which nickel ions are most stable toward further reduction to Ni(0) due to six coordination with framework oxygens,[38] whereas Ni(I) located in a main channel of clinoptilolite[25] and SAPO-41[39] is further reduced to Ni(0) by adsorbates. Our ESR results indicate that the reduction of Ni(I) to Ni(0) by methanol occurs more rapidly in mordenite than in ferrierite. This can be explained by a difference in the location and coordination of Ni(I) ions in these two materials. Ni(I) ions in a main channel of mordenite have lower coordination with only four framework oxygens, indicating less stability of these Ni(I) ions toward reduction to Ni(0) compared to Ni(I) ions situated in a ferrierite cage (site A) where they are coordinated with six framework oxygens.

Formation of paramagnetic Ni(I) has been studied previously in other zeolites and SAPO materials.[25−27,39−41] The reducibility of Ni(II) in these materials was dependent on the location and environment of the Ni(II), the Si/Al ratio, and the accessibility of Ni(II) to reducing agents. Our experimental results show that Ni(II) in NiNaK-ferrierite is more easily reduced to Ni(I) than it is in NiNaK-mordenite. This is mainly ascribed to the lesser negative charge of the ferrierite framework. According to electronegativity equalization, the reducibility of Ni(II) should decrease with decreasing electronegativity of the zeolite.[40] This is evident from a previous observation that Ni(II) in Y zeolite (Si/Al > 2) reduces easier than in X zeolite (Si/Al < 1.5) with the same Ni content.[40]

The interaction of NO has been observed in several zeolites[25,34] and SAPO materials[24,41] containing Ni(II) ions. Two kinds of paramagnetic species observable by ESR are generally formed at room temperature. One is a Ni(I)$-NO^+$ complex formed by reduction of Ni(II) by NO.[42] The other species is NO observable by ESR. NO is ESR observable only when the degeneracy of its π orbitals is removed. NO gas itself is ESR silent due to cancellation between the orbital magnetic moment and the spin magnetic moment of the electron.[33,34] The degeneracy of the π orbitals is lifted by the electric field in several zeolites and SAPO materials.[24,25,34,41] For example, when Y zeolite and clinoptilolite were treated with NO, the corresponding ESR spectra showed signals assigned to NO which were characterized by reversed **g** tensors ($g_\perp > g_\parallel$) and a triplet splitting of the $g_\perp$ component.[25,34]

Accordingly, adsorption of NO on Ni^{II}NaK-mordenite produces ESR observable NO as well as a Ni(I)$-NO^+$ complex. However, ferrierite only produces Ni(I)$-NO^+$ upon NO adsorption. Adsorption of NO on Ni^{II}NaK-ferrierite also gives an isotropic species which is already present before NO addition and was previously assigned to a Ni(I) complex with oxygen. Note that this radical species has been observed all through these experiments with various adsorbates in ferrierite, indicating that this radical species is strongly bound to the ferrierite framework. The absence of NO observable by ESR in ferrierite suggests that its crystal field is not sufficient to remove the degeneracy of the NO π orbitals.

Conclusions

This work shows comparative ESR studies on the reducibility of Ni(II), the location of Ni(I), and its interaction with several adsorbates between NiNaK-ferrierite and NiNaK-mordenite. Upon thermal and hydrogen reduction, the reducibility of Ni(II) in NiNaK-ferrierite is higher than observed in NiNaK-mordenite. This is mainly attributed to the lesser negative charge of the ferrierite framework. Thermal and hydrogen reduction produce isolated Ni(I) in both ferrierite and mordenite with somewhat different ESR parameters. Also, the interaction of Ni(I) with various sizes of adsorbates differs between ferrierite and mordenite, indicating different locations of Ni(I) in these two materials.

Molecules smaller than methanol, such as carbon monoxide and ammonia, interact with all of the Ni(I) in both ferrierite and mordenite to give the corresponding complexes, whereas for larger methanol and ethylene adsorbates, ferrierite and mordenite show differences. Ni(I) in ferrierite is situated in a site which is less accessible to methanol and ethylene and is more stable toward further reduction to Ni(0) compared to that of Ni(I) in mordenite. Upon adsorption of butene and pyridine, ferrierite shows no new ESR signal while mordenite produces a new signal due to a Ni(I) complex. From these various observations, we suggest that Ni(I) in ferrierite is situated in site A in a ferrierite cage and that Ni(I) in mordenite is located at sites in its main 12-ring channel.

Acknowledgment. This research was supported by the National Science Foundation, the Robert A. Welch Foundation, and the Korea Science and Engineering Foundation through the Advanced Materials Research Center for a Better Environment at Taejon National University of Technology.

References and Notes

(1) Li, Y.; Slager, T. L.; Armor, J. N. *J. Catal.* **1994**, *150*, 388.
(2) Li, Y.; Armor, J. N. *J. Chem. Soc., Chem. Commun.* **1997**, 2013.

(3) Iwamoto, M.; Yahiro, H.; Tanda, K.; Mizuno, N.; Mine, Y.; Kagawa, S. *J. Phys. Chem.* **1991**, *95*, 3727.
(4) Wichterlová, B.; Dedecek, J.; Sobalík, Z.; Vondrová, A.; Klier, K. *J. Catal.* **1997**, *169*, 194.
(5) Yashima, T.; Ushida, Y.; Ebisawa, M.; Hara, N. *J. Catal.* **1975**, *36*, 320.
(6) Riekert, L. *J. Catal.* **1970**, *19*, 8.
(7) Kazansky, V. B.; Elev, I. V.; Shelimov, B. N. *J. Mol. Catal.* **1983**, *21*, 265.
(8) Attfield, M. P.; Weigel, S. J.; Cheetham, A. K. *J. Catal.* **1997**, *172*, 274.
(9) Lamberti, C.; Bordiga, S.; Zecchina, A.; Salvalaggio, M.; Geobaldo, F.; Otero Areán, C. *J. Chem. Soc., Faraday Trans.* **1998**, *94*, 1519.
(10) Dedecek, J.; Wichterlová, B. *J. Phys. Chem. B* **1999**, *103*, 1462.
(11) Kaucky, D.; Dedecek, J.; Wichterlová, B. *Microporous Mesoporous Mater.* **1999**, *31*, 75.
(12) Rabo, J. A.; Angell, C. L.; Kasai, P. H.; Shoemaker, V. *Discuss. Faraday Soc.* **1966**, *41*, 328.
(13) Hartmann, M.; Azuma, N.; Kevan, L. *J. Phys. Chem.* **1995**, *99*, 10988.
(14) Oliver, D.; Richard, M.; Che, M.; Bonson-Verduraz, F.; Clarkson, R. B. *J. Phys. Chem.* **1980**, *84*, 420.
(15) Wise, W. S.; Tschernich, R. W. *Am. Mineral.* **1976**, *61*, 60.
(16) Whittemore, O. J. *Am. Mineral.* **1972**, *57*, 1146.
(17) Vaughan, P. A. *Acta Crystallogr.* **1966**, *21*, 983.
(18) Gottardi, G.; Galli, E. *Natural Zeolites*; Springer-Verlag: Berlin, 1985; p 409.
(19) Shiokawa, K.; Ito, M.; Itabashi, K. *Zeolites* **1989**, *9*, 170.
(20) Meier, W. M.; Olson, D. H. *Atlas of Zeolite Structure Types*; Butterworth: London, 1987.
(21) Kim, T. J.; Ahn, W. S.; Hong, S. B. *Microporous Mater.* **1996**, *7*, 35.
(22) Weigel, S. J.; Gabriel, J. C.; Puebla, E. G.; Bravo, A. M.; Henson, N. J.; Bull, L. M.; Cheetham, A. K. *J. Am. Chem. Soc.* **1996**, *118*, 2427.
(23) Schoonheydt, R. A.; Roodhooft, D. *J. Phys. Chem.* **1986**, *90*, 6319.
(24) Djieugoue, M. A.; Prakash, A. M.; Kevan, L. *J. Phys. Chem. B* **1999**, *103*, 804.
(25) Choo, H.; Prakash, A. M.; Park, S. K.; Kevan, L. *J. Phys. Chem. B* **1999**, *103*, 6193.
(26) Prakash, A. M.; Hartmann, M.; Kevan, L. *J. Chem. Soc., Faraday Trans.* **1994**, *89*, 3895.
(27) Michalik, J.; Narayara, M.; Kevan, L. *J. Phys. Chem.* **1984**, *88*, 5236.
(28) Ghosh, A. K.; Kevan, L. *J. Phys. Chem.* **1990**, *94*, 1953.
(29) Yu, J. S.; Kevan, L. *Langmuir* **1995**, *11*, 1617.
(30) Yu, J. S.; Kevan, L. *J. Chem. Soc., Faraday Trans.* **1995**, *91*, 3987.
(31) Back, G. H.; Yu, J. S.; Kurshev, V.; Kevan, L. *J. Chem. Soc., Faraday Trans.* **1994**, *89*, 3895.
(32) Yu, J. S.; Comets, J. M.; Kevan, L. *J. Phys. Chem.* **1993**, *97*, 10433.
(33) Lunsford, J. H. *J. Phys. Chem.* **1968**, *72*, 4163.
(34) Kasai, P. K.; Bishop, R. J. *J. Am. Chem. Soc.* **1972**, *94*, 5560.
(35) Gramlich-Meier, R.; Meier, W. M.; Smith, B. K. *Z. Kristallogr.* **1984**, *169*, 201.
(36) Mortier, W. J. *J. Phys. Chem.* **1977**, *81*, 1334.
(37) Attfield, M. P.; Weigel, S. J.; Cheetham, A. K. *J. Catal.* **1997**, *170*, 227.
(38) Feeley, J. S.; Sachtler, W. M. H. *Zeolites* **1990**, *10*, 738.
(39) Prakash, A. M.; Wasowicz, T.; Kevan, L. *J. Phys. Chem.* **1996**, *100*, 15947.
(40) Jacobs, P. A. *Catal. Rev. Sci. Eng.* **1982**, *24*, 415.
(41) Djieugoue, M. A.; Prakash, A. M.; Zhu, Z.; Kevan, L. *J. Phys. Chem. B* **1999**, *103*, 7277.
(42) Naccache, C.; Taarit, Y. *J. Chem. Soc., Faraday Trans.* **1973**, *69*, 1475.